Memory Effect on Spinodal Decomposition. 1. Effect of Uniaxial Compression

Takeji Hashimoto* and Tatsuo Izumitani†

Department of Polymer Chemistry, Graduate School of Engineering, Kyoto University, Kyoto 606-01, Japan

Received February 20, 1996; Revised Manuscript Received August 20, 1996[⊗]

ABSTRACT: Effects of a uniaxial compression on the phase-separation process of a binary mixture of poly(styrene-*ran*-butadiene) (SBR) and polybutadiene (PB) were studied by means of time-resolved light scattering. For this purpose, the uniaxial compression of $\gamma_p = 1$ to 0.25 was imposed on the film which was first subjected to isothermal phase separation in the absence of external deformations. The scattering intensity distributions were detected as a function of scattering vector **q** in the plane perpendicular to the compression axis with the incident beam parallel to the compression axis. After the compression, the scattering vector at a maximum intensity $q_m(\gamma_p)$ abruptly decreased with γ_p nearly in accord with affine deformation. In an earlier time after the compression, the peak scattering vector $q_m(t;\gamma_p)$ remained unchanged with time t for a certain time period and then decreased in the same manner as that found for the phase separation in the undeformed sample, indicating that a memory effect of the uniaxial compression decays with time. Cahn's linear analysis after the uniaxial compression in the time range where $q_m(t;\gamma_p)$ was constant indicated that the growth rate $R(q,\gamma_p)$ of the concentration fluctuations with wave number q depends strongly on γ_p, clearly revealing that the growth process is nonlinear, depending on the initial state. The effect of the uniaxial compression on the late stage spinodal decomposition was also analyzed: the scaled structure factors perpendicular to the compression axis were determined as a function of γ_p. The results indicated that the global scaled structure factor was almost identical to that found for the undeformed case, although the local structure was affected by the uniaxial compression.

I. Introduction

Studies of phase-separation kinetics are current topics from both industrial and academic points of view. Over the past decade, a number of studies have been made on the coarsening kinetics of the phase-separated structure of polymer mixtures.[1] The results have shown that the coarsening process of the polymer mixtures with a critical composition can be classified into the following three stages: (i) early stage, (ii) intermediate stage, and (iii) late stage. In the early stage of spinodal decomposition (SD), the time evolution of concentration fluctuations is well-described by the linearized theory proposed by Cahn for small molecule systems,[2] and the concentration fluctuations grow exponentially with time. In the intermediate stage of SD, the time evolution of the concentration fluctuations becomes increasingly nonlinear with time, and as a consequence, both the wavelength and amplitude of the dominant mode of concentration fluctuations grow with time. In the late stage of SD, the amplitude of concentration fluctuations reaches an equilibrium value, but the size of the phase-separated structure keeps growing with time.[3]

Recently, Jinnai et al.[4] reported the memory effect of the initial thermal concentration on the early stage SD for a mixture of deuterated polybutadiene and protonated polybutadiene measured by small angle neutron scattering (SANS). They concluded that the thermal concentration fluctuations present in the system before the onset of the SD do affect both the early stage SD and the early phase of the intermediate stage SD, giving rise to the memory effect on the time evolution of the characteristic wave number $q_m(t)$ and the maximum scattered intensity $I_m(t)$ and hence on the ordering process. However, the effect was not strong enough to alter the q-dependent growth rate of the concentration fluctuations in the Cahn−Hilliard−Cook (CHC) theory,[2] and the early stage SD could still be treated in terms of the CHC theory.

The present paper reports a new approach for investigating the effects of the initial concentration fluctuations on the subsequent SD process. In this approach we first develop a phase-separated structure in the system which belongs to the intermediate stage SD. Subsequently we impose uniaxial compression of various compression ratios (γ_p) to the system in order to set up various initial concentration fluctuations for a further progress of the phase separation. We then investigate the SD process which develops under these well-controlled initial conditions. In this way we can select a much wider spectrum of concentration fluctuations, both in terms of length scale and amplitude, as an initial condition, than the previous study,[4] which may facilitate explorations of the intrinsically nonlinear nature of the ordering process via SD. The aim of this study is to contribute to our understanding of the nonlinear dynamics in the ordering process of thermodynamically unstable systems.

II. Experimental Methods

II.A. Samples. Polybutadiene (PB) and poly(styrene-*ran*-butadiene) (SBR) were polymerized by living anionic polymerization and had a narrow molecular weight distribution. SBR contains 80 wt % butadiene and had a number average molecular weight (M_n) of 1.00×10^5 and $M_w/M_n = 1.18$ (M_w being the weight average molecular weight). PB has $M_n = 1.60 \times 10^5$ and $M_w/M_n = 1.16$. Fractions of cis, trans, and vinyl linkages of the butadiene part as measured by infrared spectroscopy are 0.16, 0.23, and 0.61 for SBR and 0.19, 0.35, and 0.46 for PB.

II.B. Preparation of Mixture. Binary mixtures of SBR/PB = 70/30 (v/v) were dissolved into a dilute solution of toluene (7 wt % polymer solution). The 0.15 mm thick film specimens were obtained by evaporating the solvent at a natural rate at about 25 °C in a Petri dish. The film specimens thus obtained

† Present address: Daicel Chemical Industries Ltd., 1239 Shinzaike, Aboshi-ku, Himeji, Hyogo 671-12, Japan.

⊗ Abstract published in *Advance ACS Abstracts,* November 1, 1996.

S0024-9297(96)00264-1 CCC: $12.00

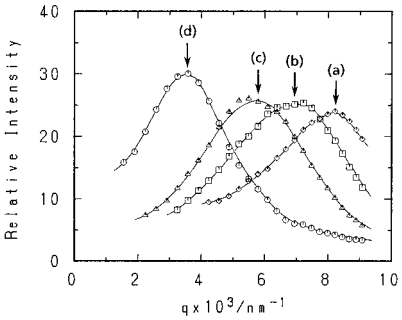

Figure 1. Light scattering profile for a film that was first homogenized and then demixed by annealing at 60 °C for 31 min ($\gamma_p = 1$) (a) and its change with the uniaxial compression at 60 °C with the compression ratio of $\gamma_p = 0.68$ (b), 0.50 (c), and 0.25 (d).

were then dried under vacuum for more than 1 week at room temperature.

The film specimens thus prepared were further homogenized by applying "Baker's transformation" at room temperature, i.e., by applying repeated folding and pressing over many times, as reported earlier.[5] The homogenized specimens were quickly sandwiched between two glass plates with a spacer of an appropriate thickness and were subjected to the light scattering experiments.

II.C. Methods of Uniaxial Compression. The uniaxial compression was performed on films (designated as *as-prepared film specimens*) which were first subjected to the homogenization process and then to isothermal demixing for 31 min at 60 °C, followed by rapid cooling to 25 °C. The as-prepared film was compressed at 25 °C, unless stated otherwise, after rapidly changing a spacer to a thinner spacer with an appropriate thickness by putting a weight of 10 kg on the top of the glass plates. The compression ratio γ_p was defined as the ratio of sample thickness after the compression (d) to that before the compression (d_0).

$$\gamma_p = d/d_0 \tag{1}$$

The weight was then released, and the samples were immediately used for light scattering experiments. The time spent between the demixing process at 60 °C and the compression process and that between the compression process and the onset of the light scattering experiment after the compression are negligibly short compared with the time scale of the SD process. Thus, these time periods hardly affect the results we discuss here. There was no recovery in the sample dimension after the removal of the weight. The stress was relaxed completely before the new folding−pressing was applied in the Baker's transformation process and before the light scattering measurements were performed after compression.

II.D. Methods of Observation. The phase-separating structure was investigated in real time by means of the time-resolved light scattering technique. A 15 mW He−Ne laser ($\lambda = 632.8$ nm) was used as an incident beam source. The compressed film was set into a metal block with two windows for the incident and scattered beams and preheated at a demixing temperature of 60 °C. The incident beam was parallel to the film normal and hence the compression axis. The scattering profiles were observed on the detector plane set perpendicular to the incident beam. Thus, the scattering vector **q** is approximately perpendicular to the uniaxial compression axis.

III. Experimental Results

III.A. Effects of Uniaxial Compression on Phase-Separated Domains. Figure 1 shows the light scattering profile from the as-prepared film which was first homogenized and demixed at 60 °C for 31 min (profile a) together with those from the as-prepared films

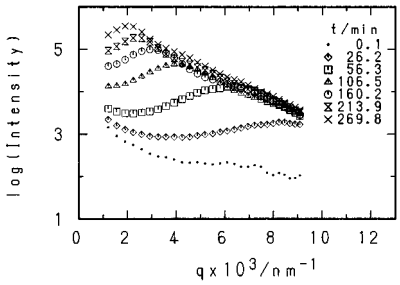

Figure 2. Time evolution of the scattering profiles on a semilogarithmic scale during isothermal demixing at 60 °C for the homogenized film. The time $t = 0$ was taken immediately after the homogenization process.

subsequently subjected to the uniaxial compression at 60 °C; $\gamma_p = 0.68$ (b), 0.50 (c), and 0.25 (d). The scattering maximum arising from a periodic concentration fluctuation, which was developed in the homogenized films via SD process, shifts toward a smaller q with the compression, indicating the phase-separated domains expanded in the direction perpendicular to the uniaxial compression axis. The compression was imposed to the film in a few minutes. This time is much shorter than that of the structural evolution driven by the thermodynamic driving force but is longer than that for stress relaxation and for the relaxation of molecular orientation.

III.B. Time Evolution of Scattering Profile after Uniaxial Compression. Figure 2 shows the time evolution of light scattering profiles at 60 °C from the films after the homogenization but without compression ($\gamma_p = 1$). As time elapses, a scattering maximum appears, the maximum intensity increases, and the scattering vector q_m at the maximum intensity shifts toward small q. Here, the scattering vector **q** is defined later in eq 3. This phenomenon which reflects the coarsening of phase-separated domains was well-described earlier.[6,7]

Figure 3 shows the time evolution of light scattering profiles for the compressed films at 60 °C with $\gamma_p = 0.68$ (a), 0.50 (b), and 0.25 (c). The time t was set equal to zero right after the homogenization and the onset of the phase separation at 60 °C. The films were first homogenized and then subjected to isothermal demixing at 60 °C for 31 min, followed by quenching to 25 °C. Then, the films were uniaxially compressed and quickly transferred to the heated block precontrolled at 60 °C for further phase separation. In these figures, the time change in the scattering profiles from 0.1 to 31.1 min (curves 1−4) corresponds to that in the undeformed state. Thus, the scattering profiles at a time of 31.1 min (profile 4) are those obtained immediately before the uniaxial compression. After the uniaxial compression is imposed, the following changes in the scattering profile were observed: (a) the scattering maximum shifts toward a smaller q value without a significant change in the maximum intensity (from profile 4 to profile 5 in Figure 3); (b) at the beginning of the phase separation process after the compression, the scattering intensity increases with time without a significant change in the scattering vector q_m at the maximum intensity.

IV. Analysis and Discussion

The scattered intensity at scattering vector **q** and time t from the phase-separating structure is generally given by

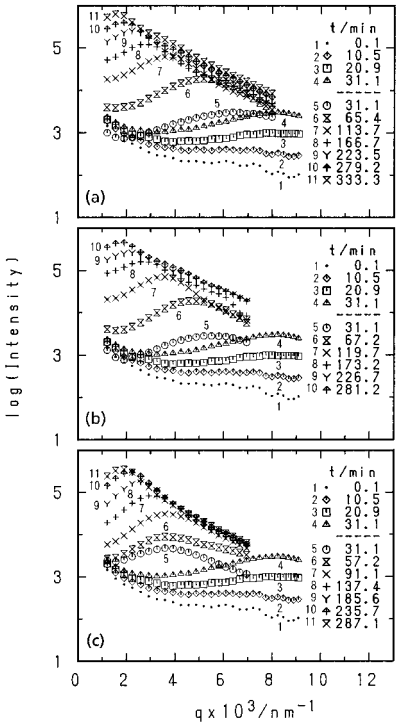

Figure 3. Time evolution of the scattering profiles for the compressed films with $\gamma_p = 0.68$ (a), 0.50 (b), and 0.25 (c) at 60 °C. The films were first homogenized and then subjected to the time-resolved LS experiment from 0.1 to 31.1 min at 60 °C (time zero is set right after the homogenization, i.e., the onset of SD at 60 °C), followed by quenching to 25 °C, where the uniaxial compression was imposed on the film, and finally quickly transferred back to the block controlled at 60 °C for further phase separation and the time-resolved LS experiments. The scattering profile at 31.1 min (profile 5 shown by circles) is immediately after the uniaxial compression, while profile 4 shown by triangles is immediately before the compression.

$$I(\mathbf{q},t) = I(q_x,q_y,q_z,t) = K_1\langle\eta^2\rangle\Lambda_x\Lambda_y\Lambda_z S(q_x/q_{mx},q_y/q_{my},q_z/q_{mz},t) \quad (2)$$

where the magnitude of $\mathbf{q}$ is defined by

$$q = (4\pi/\lambda)\sin(\theta/2) \quad (3)$$

with λ and θ being the wavelength of light and the scattering angle, respectively, both in the medium. K_1, $\langle\eta^2\rangle$, and $S(q_x/q_{mx},q_y/q_{my},q_z/q_{mz},t)$ are a proportionality constant, the mean-squared refractive index fluctuation of our systems, and a scaling function characterizing the shape of our structure at a given time, respectively. The q_k and q_{mk} are components of the scattering vector $\mathbf{q}$ and characteristic scattering vector $\mathbf{q}_m$ (the scattering vector at maximum scattered intensity) in the kth direction ($k = x, y, z$), respectively. Λ_k is a characteristic length of the structure along the kth direction defined by

$$\Lambda_k = 2\pi/q_{mk}, \quad k = x, y, z \quad (4)$$

We define the Cartesian coordinate O_{xyz}, in which the O_z axis is normal to the film surface O_{xy} and parallel to the axis of the uniaxial compression and to the propagation direction of the incident beam (see Figure 4). We observe the scattered intensity distribution $I_\perp(q_x,q_y,t)$ in the detector plane set normal to the O_z axis:

$$I_\perp(q_x,q_y,t) \equiv I(q_x,q_y,q_z=0,t) = K_2\langle\eta^2\rangle q_{mx}^{-1} q_{my}^{-1} q_{mz}^{-1} S_\perp(q_x/q_{mx},q_y/q_{my},t) \quad (5)$$

with

$$S_\perp(q_x/q_{mx},q_y/q_{my},t) \equiv S(q_x/q_{mx},q_y/q_{my},q_z/q_{mz}=0,\ t) \quad (6)$$

Under the uniaxial compression,

$$\Lambda_x = \Lambda_y \equiv \Lambda_\perp \quad (7)$$

$$q_{mx} = q_{my} = q_{m\perp} \quad (8)$$

$$\Lambda_\perp = 2\pi/q_{m\perp} \quad (9)$$

and

$$\Lambda_z \equiv \Lambda_{||} \quad (10)$$

$$q_{mz} = q_{m||} \quad (11)$$

$$\Lambda_{||} = 2\pi/q_{m||} \quad (12)$$

We note that the scattered intensity distribution in the detector plane is circularly symmetric with respect to the incident beam axis,

$$I_\perp(q_x,q_y,t) = I_\perp(q_\perp,t) = K_2\langle\eta^2\rangle q_{m\perp}^{-2}(t)\, q_{m||}^{-1}(t)\, S_\perp(q_\perp/q_{m\perp},t) \quad (13)$$

where

$$q_\perp \equiv (q_x^2 + q_y^2)^{1/2} \quad (14)$$

IV.A. Effect of Uniaxial Compression on the Scattering Pattern. Here, we attempt to predict effects of the uniaxial compression on the domain structure developed by SD on the basis of affine deformation. The characterization of the structure (the concentration fluctuations) right after the compression is important in order to identify the initial conditions for a further progress of the phase separation after the compression. From eq 13, the static scattering pattern immediately after the uniaxial compression is described by

$$I_\perp(q_\perp) = K_2\langle\eta^2\rangle q_{m\perp}^{-2} q_{m||}^{-1} S_\perp(x) \quad (15)$$

with

$$x \equiv q_\perp/q_{m\perp} \quad (16)$$

The integrated intensity on the detector plane $Q_\perp$ is given by

$$Q_\perp \equiv \int_0^\infty I_\perp(q_\perp) q_\perp \, dq_\perp = K_2\langle\eta^2\rangle q_{m||}^{-1}\int_0^\infty S_\perp(x)x\, dx = K_3\langle\eta^2\rangle q_{m||}^{-1} \quad (17)$$

where K_3 is a constant. The scaled structure factor $F_\perp(x)$ on the detector plane is given by

$$F_\perp(x) \equiv I_\perp(x) q_{m\perp}^{-2} = K_2\langle\eta^2\rangle q_{m||}^{-1} S_\perp(x) \quad (18)$$

$$\int_0^\infty F_\perp(x)x\, dx = K_3\langle\eta^2\rangle q_{m||}^{-1} \quad (19)$$

On the other hand, the static scattering pattern from the isotropic structure, i.e., undeformed structure, is

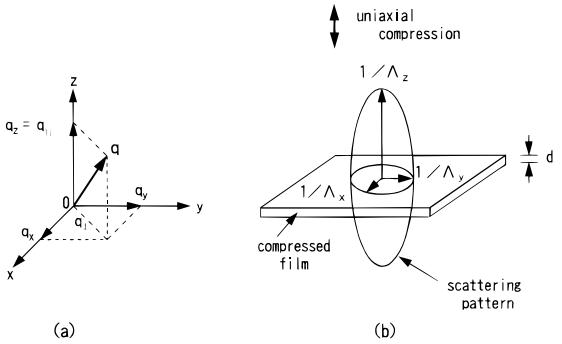

Figure 4. Coordinate system used in this work.

defined by

$$I(q) = K_2\langle\eta^2\rangle q_{m0}^{-3} S(x) \tag{20}$$

with

$$x \equiv q/q_{m0} \tag{21}$$

where q_{m0} is the characteristic wave number for the undeformed structure ($\gamma_p = 1$), and $S(x)$ is the scaling function for the undeformed structure. The corresponding integrated intensity on the detector plane $Q_\perp$ is given by

$$Q_\perp \equiv \int_0^\infty I(q_\perp) q_\perp \, dq_\perp = K_2\langle\eta^2\rangle q_{m0}^{-1} \int_0^\infty S(x) x \, dx = K_3\langle\eta^2\rangle q_{m0}^{-1} \tag{22}$$

The scaled structure factor for the undeformed structure is defined by

$$F_{\perp 0}(x) \equiv I_\perp(x) q_{m0}^{\,2} = K_2\langle\eta^2\rangle q_{m0}^{-1} S(x) \tag{23}$$

similar to that for the deformed structure (eq 18). Note that this definition is different from the conventional definition ($F(x) \equiv I(x) q_{m0}^{\,3}$).

$$\gamma_p = \Lambda_\parallel/\Lambda_0 \tag{24a}$$

$$= q_{m0}/q_{m\parallel} \tag{24b}$$

where Λ_0 is the characteristic length before the uniaxial compression. If the change of the spacing obeys isochoric affine deformation

$$\Lambda_\perp/\Lambda_0 = \gamma_p^{-1/2} \tag{25}$$

The value Λ_0 and $\Lambda_\perp$ as a function of γ_p can be estimated from the peak scattering vectors q_{m0} and $q_{m\perp}(\gamma_p)$ in the profiles shown in Figure 1 and from eq 9: they are 0.76, 0.91, 1.1, and 1.8 μm for $\gamma_p = 1$, 0.68, 0.5, and 0.25, respectively. Figure 5 shows the plot of log-($\Lambda_\perp/\Lambda_0$) versus log γ_p. The solid line indicates the relation for the isochoric affine deformation with slope $-1/2$. The expansion of the spacing normal to the compression axis seems to obey approximately the isochoric affine deformation (result 1), though it is slightly greater than that predicted by the affine deformation for a larger compression deformation: its reason was already discussed elsewhere.[5] From eqs 17 and 24b, the measured integrated intensity on the plane normal to the compression axis $Q_\perp(\gamma_p)$ is given by

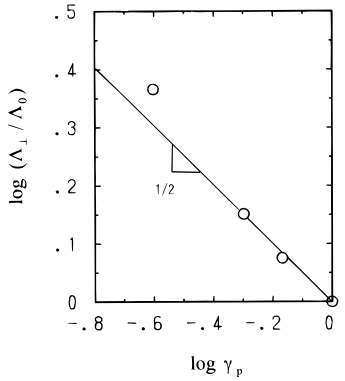

Figure 5. $\Lambda_\perp/\Lambda_0$ versus γ_p on a double logarithmic scale. The solid line indicates isochoric affine deformation with the slope of $-1/2$.

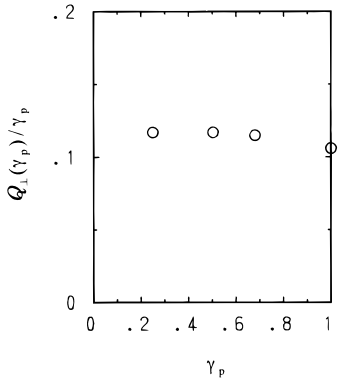

Figure 6. Reduced integrated intensity $Q_\perp(\gamma_p)/\gamma_p$ vs γ_p.

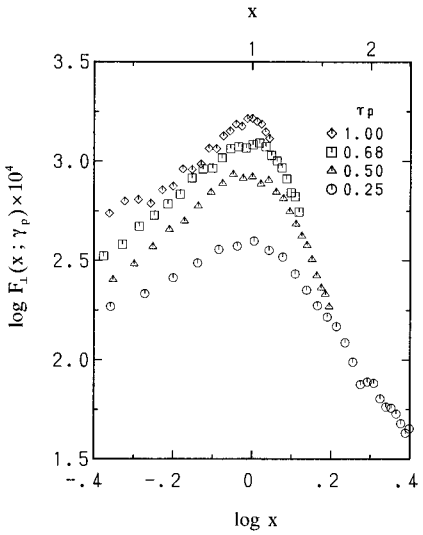

Figure 7. Scaled structure factors $F_\perp(x;\gamma_p)$ on a double logarithmic scale measured immediately after the uniaxial compression with various γ_p's at 60 °C.

$$Q_\perp(\gamma_p) \cong \int_{q_{\perp min}}^{q_{\perp max}} I_\perp(q_\perp) q_\perp \, dq_\perp = K_3\langle\eta^2\rangle\gamma_p q_{m0}^{-1} \tag{26}$$

Here $q_{\perp max}$ and $q_{\perp min}$ are respectively the magnitude of the scattering vector $q_\perp$ above and below which the integrand goes effectively to zero.

Figure 6 shows $Q_\perp(\gamma_p)/\gamma_p$ as a function of γ_p. The results indicate that the mean-squared refractive index fluctuation $\langle\eta^2\rangle$ is almost unchanged with the compression over the range of γ_p covered in this experiment (result 2). $x_{max} \equiv q_{\perp max}/q_{m\perp}$ and $x_{min} \equiv q_{\perp min}/q_{m\perp}$ taken are 0.5 and 1.5, respectively.

Figure 7 shows the scaled structure factor $F_\perp(x)$ against the reduced wave number x on a double loga-

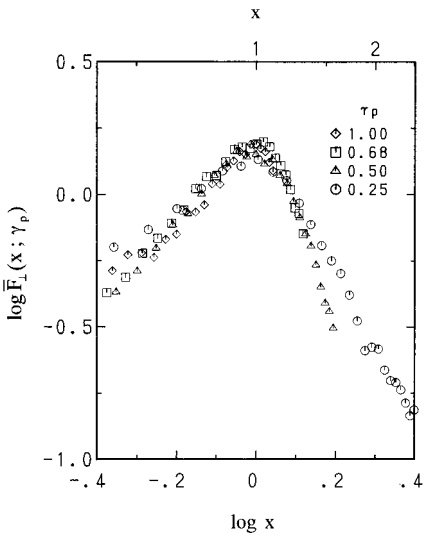

Figure 8. Reduced scaled structure factor $\bar{F}_\perp(x;\gamma_p)$ on a double logarithmic scale measured immediately after the uniaxial compression at various γ_p's and at 60 °C.

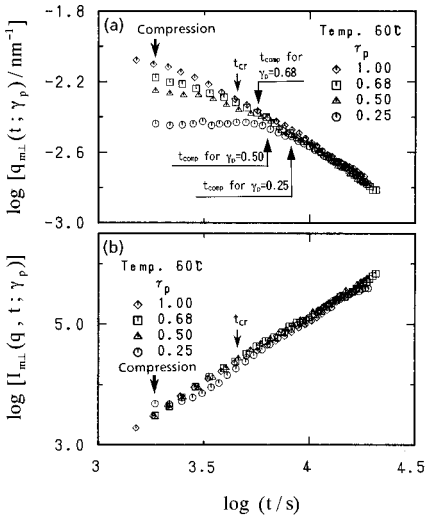

Figure 9. Time changes in the scattering vector $q_{m\perp}(t;\gamma_p)$ at the maximum intensity (a) and the peak scattered intensity $I_{m\perp}(t;\gamma_p)$ (b) on a double logarithmic scale from films subjected to the uniaxial compression with various γ_p's at 60 °C and at a time indicated by the arrow marked "Compression".

rithmic scale for $\gamma_p = 1$ (diamonds, undeformed), 0.68 (squares), 0.50 (triangles), and 0.25 (circles). The intensity of the scaled structure factor tends to decrease with the compression deformation, i.e., decreasing γ_p. Judging from the result obtained in Figure 6 and from eq 18, this is interpreted to be primarily due to a decrease of $q_{m||}^{-1}$ with the compression deformation.

From eqs 18, 25, and 26 a reduced scaled structure factor $\bar{F}_\perp(x)$

$$\bar{F}_\perp(x) \equiv F_\perp(x)/Q_\perp(\gamma_p) \tag{27}$$

is given by

$$\bar{F}_\perp(x) = (K_2/K_3)S_\perp(x) \tag{28}$$

Figure 8 shows the reduced scaled structure factor $\bar{F}_\perp(x)$ against x on a double logarithmic scale. The reduced scaled structure factor is found to be approximately universal with γ_p for $\gamma_p \geq 0.5$, i.e., for a small degree of compression deformation. A slight broadening was observed for a large degree of compression such as $\gamma_p \leq 0.25$. Thus, not only the spacing but also the structure itself tends to be deformed affinely upon the compression deformation (result 3). The structure factor itself reveals the bicontinuous phase-separated domain structure as describe earlier.[8,9] However at the large deformation of $\gamma_p \leq 0.25$, the structures are significantly broadened.

The results in Figures 6−8 suggest that (i) the domain structure normal to the compression axis is approximately scaled with the single length parameter $q_{m\perp}^{-1}$ over the range of γ_p covered in this experiment with $q_{m\perp}$ changing with γ_p according to the isochoric affine deformation (results 1 and 3) and that (ii) $\langle\eta^2\rangle$ is almost unchanged with the compression (result 2). The characteristic length scale $\Lambda_\perp$ changes from 0.76 to 1.8 μm and $\Lambda_{||}$ changes from 0.76 to 0.14 μm with decreasing γ_p from 1 to 0.25.

IV.B. Phase Separation after Uniaxial Compression: Time Evolution of the Characteristic Wave Number. Figure 9a shows the time changes in the scattering vector $q_{m\perp}(t;\gamma_p)$ at the maximum intensity measured at 60 °C for the undeformed case (diamonds) ($\gamma_p = 1$) and for deformed films with $\gamma_p = 0.68$ (squares), 0.50 (triangles), and 0.25 (circles) on a double logarithmic scale. The crossover time t_{cr} is explained later in the text. The time evolution of the scattering function for the undeformed case was well-described in our earlier study.[7] The scattering vector $q_{m\perp}(t;\gamma_p)$ for the deformed films abruptly decreases toward a smaller q by the uniaxial compression applied at a time as indicated by an arrow marked with "compression" and then slowly decreases or remains unchanged with time until a certain time defined as t_{comp} at which $q_{m\perp}(\gamma_p=1;t=t_{comp}) \cong q_{m\perp}(\gamma_p<1;t=t_{comp})$. The value $q_{m\perp}(t;\gamma_p)$ then decreases with t at the same rate as the value $q_{m\perp}(t;\gamma_p=1)$ decreases. The changes in $q_{m\perp}$ with time correspond to those in $\Lambda_\perp$ from 0.80 to 3.9 μm (see eq 9). The time t_{comp} appears to depend on γ_p; the larger the degree of compression, the longer the time t_{comp}. Thus, the memory effect of the uniaxial compression decays during the ordering process after the compression at the level of $q_{m\perp}(\gamma_p=1) \cong q_{m\perp}(\gamma_p<1)$, and thereafter the coarsening depends purely on temperature (result 4).

The trend as described above is consistent with that found by the computer simulation by Takenaka et al.[8] They reported a computational study on the effect of a $^1/_2$-uniaxial compression on the ordering process via SD based on the time-dependent Ginzburg−Landau equation. They found that the characteristic wave number $q_{m||}(t)$ shifts to higher q after the compression, and then the time change in $q_{m||}(t)$ approaches that of the case without the compression. On the other hand, $q_{m\perp}(t)$ first shifts to the lower q by the compression, then it is kept almost constant with time after the compression, and finally the time change in $q_{m\perp}(t)$ approaches that in $q_{m0}(t)$ without the compression. They also found that the relaxation parallel to the compression axis is much faster than that perpendicular to it. This anisotropy in the relaxation behavior can be understood as a consequence of the fact that the modes having higher q have a higher energy and hence a stronger thermodynamic driving force for the decay than those having lower q.

Figure 9b shows the time changes of the maximum scattering intensity $I_{m\perp}(t;\gamma_p)$ at 60 °C on the detector plane for the undeformed film (diamonds) ($\gamma_p = 1$) and that for deformed films with $\gamma_p = 0.68$ (squares), 0.50 (triangles), and 0.25 (circles) on a double logarithmic

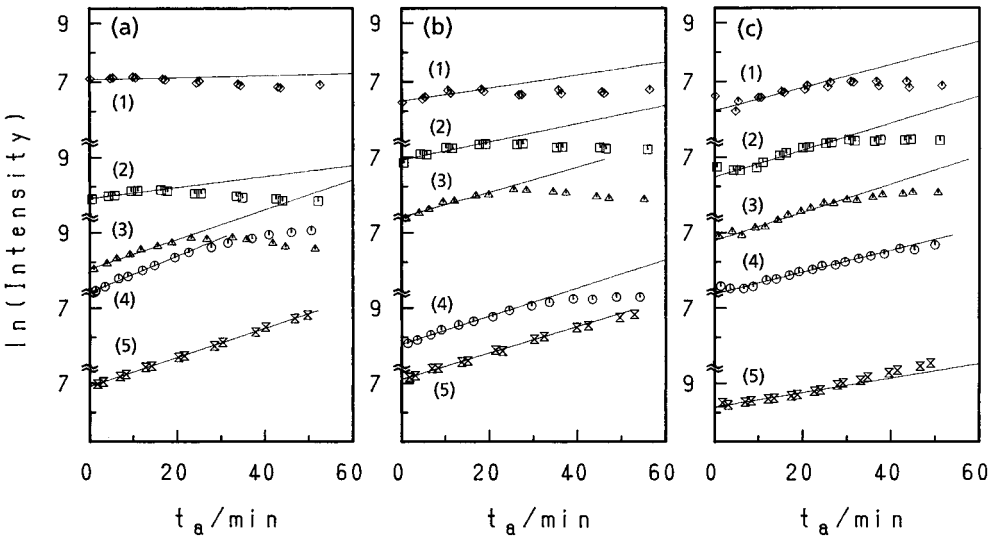

Figure 10. ln $I_\perp(q,t;\gamma_p)$ vs t_a (t_a, time after the uniaxial compression) for films subjected to the uniaxial compression at 60 °C with $\gamma_p = 0.68$ (a), 0.50 (b), and 0.25 (c).

scale. The result indicates that the maximum scattering intensity $I_{m\perp}$ was not affected by the uniaxial compression. Although the result is surprising at first glance, we can recognize that it is consistent with those given in Figure 5 (isochoric affine deformation), Figure 6 (nearly constant $\langle\eta^2\rangle$ with γ_p), and Figure 8 (nearly constant $S_\perp(x)$ with γ_p). $I_{m\perp} \equiv I_\perp(q_\perp{=}q_{m\perp})$ is not affected by γ_p, if γ_p does not alter $\langle\eta^2\rangle$ and $S_\perp(x)$ (see eq 15).

IV.C. Phase Separation after Uniaxial Compression: Linear Analysis. In the earlier time after the uniaxial compression, the characteristic wave numbers $q_{m\perp}(t;\gamma_p)$ are almost independent of time, especially at a large compression deformation ($\gamma_p = 0.25$). Thus, we tried to apply the linear analysis of SD to the time evolution of $I_\perp(q,t_a)$ in this time domain of $0 \le t_a < t_{comp}$. Hereafter, we suppress the subscript $\perp$ in $q_\perp$ and $I_\perp$ for simplicity; t_a is the time spent after the uniaxial compression. The linearized theory gives[2]

$$I_\perp(q_\perp,t_a) \equiv I(q,t_a) = I(q,t_a{=}0)\exp[2R(q)t_a] \quad (29)$$

where $R(q)$ is a growth rate of the concentration fluctuations with wave number q after the uniaxial compression and under the special initial condition characterized by $I(q,t_a{=}0)$. In a small q regime where $qR_0 \ll 1$ (R_0 being the unperturbed end-to-end distance of polymers) one can show that $R(q)$ is given by

$$R(q) = q^2 D_{app}[1 - q^2/2q_m^2(0)] \quad (30)$$

where D_{app} is the mutual diffusivity of polymer mixtures and $q_m(0)$ is the characteristic wave number (the wave number of dominant mode of concentration fluctuations). The characteristic parameters D_{app} and $q_m(0)$ of the early stage SD for the undeformed specimens were obtained in our earlier study:[6] $D_{app} = 27$ nm^2 s^{-1} and $q_m(0) = 9.3 \times 10^{-3}$ nm^{-1} at 60 °C; the characteristic time $t_c = 430$ s where t_c is defined by $t_c \equiv (q_m^2(0)D_{app})^{-1}$ at 60 °C. The time (31 min) at which the compression was imposed on the as-prepared films corresponds to the reduced time $\tau = 4.3$, where τ is defined as $\tau \equiv t/t_c$. The crossover time t_{cr} from the intermediate stage SD to the late stage SD for this system is $t_{cr} = 72$ min.[6] Therefore the uniaxial compression was imposed at an intermediate stage. Note that the crossover was found[3] to occur at $\tau \cong 10$ so that $t_{cr} = 10t_c$.

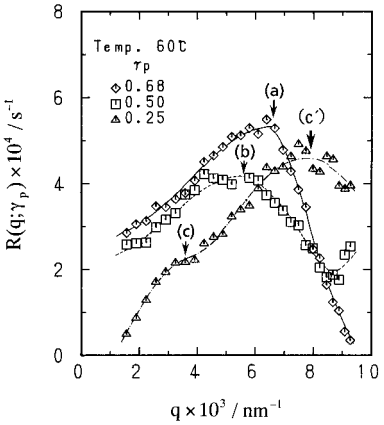

Figure 11. Growth rate of the concentration fluctuations $R(q;\gamma_p)$ as a function of q for the films subjected to the uniaxial compression at 60 °C with $\gamma_p = 0.68$ (a), 0.50 (b), and 0.25 (c). The arrows indicate a shift of the scattering vector at the maximum intensity $q_{m\perp}(\gamma_p)$ with uniaxial compression.

Figure 10 shows the variations of logarithmic scattering intensity ln $I(q,t)$ with t_a at various scattering vectors **q** during the demixing at 60 °C after the uniaxial compression for $\gamma_p = 0.68$ (a), 0.50 (b), and 0.25 (c). As shown in the figure, the scattered intensity apparently increases exponentially with time in the early stage of the ordering process after the compression over the q range covered in this experiment. One can find that the apparent linear time region (i.e., the time region where the linearized theory of eq 29 is apparently applicable) expands with an increase of the compression (result 5). The deviation of the intensity increase from the exponential behavior is seen in the later time, reflecting the shift of the scattering maximum toward smaller q due to the nonlinear nature of the ordering process. The q-dependence of the growth rate $R(q)$ in the early stage was estimated on the basis of eq 29. The results obtained at various γ_p are plotted in Figure 11.

At a small compression deformation ($\gamma_p = 0.68$) the maximum growth rate is found at $q = q_m \cong 6 \times 10^{-3}$ nm^{-1} (the arrow marked a). This maximum shifts toward smaller q with an increasing degree of the compression as shown by the arrows a−c, and the maximum growth rate decreases with an increasing degree of the compression. The values q_m shown by the arrows a−c coincide with those observed in the scatter-

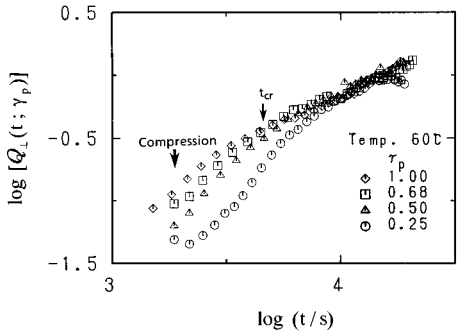

Figure 12. Changes in the integrated scattering intensity $Q_\perp(t;\gamma_p)$ with time on a double logarithmic scale for the films subjected to the uniaxial compression at 60 °C with various γ_p.

ing profiles immediately after the compression and hence reflect the growth behavior of the dominant mode of the concentration fluctuations after the deformation. We define this mode as a preexisting mode, because it existed right after the deformation and even before a further progress of the phase separation after the deformation. In addition to the growth of the dominant mode, we found that a growth of new modes of concentration fluctuations appears at higher q values, having a maximum growth rate at $q > q_m$ (see, for example, thick arrow c′ for the data obtained at $\gamma_p = 0.25$). For the data obtained at $\gamma_p = 0.50$, the new modes appear at $q > 9 \times 10^{-3}$ nm^{-1} outside the window of our observation. These new modes appear to grow in superposition of the preexisting modes of the concentration fluctuations. Thus, we obtained the following pieces of evidence on the ordering process (result 6): the growth of the new modes strongly couples with that of the preexisting modes, giving rise to a strong γ_p dependence of $R(q)$. Thus, the results clearly reveal that the growth process is intrinsically and highly nonlinear.

We next consider how the integrated intensity on the detector plane $Q_\perp(t;\gamma_p)$ changes with time during the ordering process after the compression. From eq 17 we obtained

$$Q_\perp(t;\gamma_p) = K_3\langle\eta(t)^2\rangle q_{m\|}^{-1}(t) \tag{31}$$

Note that $Q_\perp$ in eq 17 is the intensity at a time immediately after the compression. Figure 12 shows, on a double logarithmic scale, the integrated intensity $Q_\perp(t;\gamma_p)$ as a function of time for the films imposed to various γ_p. The results indicate that, at an earlier time after the uniaxial compression, the level of the $Q_\perp(t;\gamma_p)$ was affected by γ_p, namely, the larger the degree of compression, the lower the level of the $Q_\perp(t;\gamma_p)$. This is simply because $q_{m\|}$ increases but $\langle\eta^2\rangle$ is unchanged, as verified earlier in section IV.A, with the compression (see eq 26 or 31). The increase of $Q_\perp$ with time at a given γ_p is primarily due to an increase of $\langle\eta^2\rangle$ with t in the early stage; however, in the late stage the increase is only due to the increase of $q_{m\|}^{-1}$ (i.e., for the data at $\gamma_p = 1$, this regime occurs at $t > t_{cr}$). The increase of $q_{m\|}^{-1}$ corresponds to the increase of the characteristic length $\Lambda_\|$ from 1.8 μm right after the compression to 3.9 μm at the end of our experiment for the case of $\gamma_p = 0.25$ (result 7). Again the memory effect of the uniaxial compression decays at a long enough time after the uniaxial compression. As a result the coarsening process depends only the phase-separation temperature.

IV.D. Phase Separation after Uniaxial Compression: Scaled Structure Factor. Here, we analyzed

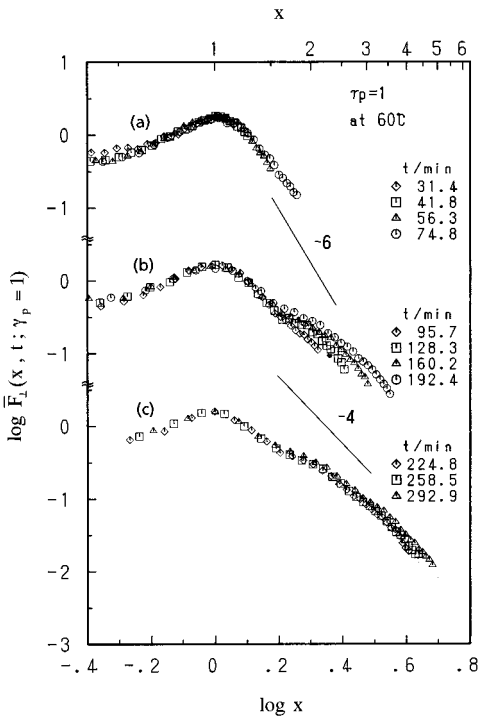

Figure 13. Reduced scaled structure factor $\bar{F}_\perp(x)$ on a double logarithmic scale at 60 °C with $x \equiv q/q_{m0}$ for the film without compression ($\gamma_p = 1$).

the scaled structure factor. The main concern here is how the scaling function changes with time after imposing the uniaxial compression. If the time evolution of the scattering profile obeys the dynamical scaling law,[11] the time evolution of the scattering function $I(q,t;\gamma_p)$ is given in terms of the universal scaling function S. The scaled structure factor on the detector plane is defined by

$$F_\perp(x,t) \equiv I_\perp(x,t)\, {q_{m\perp}}^2(t) = K_2\langle\eta(t)^2\rangle {q_{m\|}}^{-1}(t)\, S_\perp(x,t) \tag{32}$$

similarly to eq 18 (note that eq 18 defines the structure factor immediately after the compression). From eqs 31 and 32, the reduced scaled structure factors $\bar{F}_\perp(x)$ are defined as follows and given by

$$\bar{F}_\perp(x,t) \equiv F_\perp(x,t)/Q_\perp(t;\gamma_p) = (K_2/K_3)S(x,t) \tag{33}$$

similarly to eq 28.

Figure 13 shows the reduced scaled structure factor $\bar{F}_\perp$ at $\gamma_p = 1$. Note that the crossover time t_{cr} between the intermediate stage and the late stage was 72 min, so that part a corresponds to that in the intermediate stage and parts b and c to those in the late stage. Note also that even in the intermediate stage the scaled structure factor $\bar{F}_\perp$ normalized with $Q_\perp \sim \langle\eta^2\rangle$ is nearly universal with t, indicating that the global structure manifested by $\bar{F}_\perp$ at $0.5 \le x \le 1.5$ grows with the dynamical self-similarity: only $\langle\eta^2\rangle$ and the length parameter $q_{m\perp}^{-1}$ increase with time. The scaled structure factor reveals that the phase-separating domain structure is bicontinuous, as clarified earlier.[8,9] The high-order maximum was observed at $x \cong 2$ in parts b and c. $\bar{F}_\perp(x)$ has the asymptotic behavior x^n with $n \cong -6$ in a range of $1 < x < 2$ and $n = -4$ in a range of $x > 2$ as described earlier.[9] The domains with a sufficiently uniform spatial periodicity are essential to the high-order peak in $\bar{F}_\perp(x)$ at $x \cong 3$. The increase of $\bar{F}_\perp(x)$

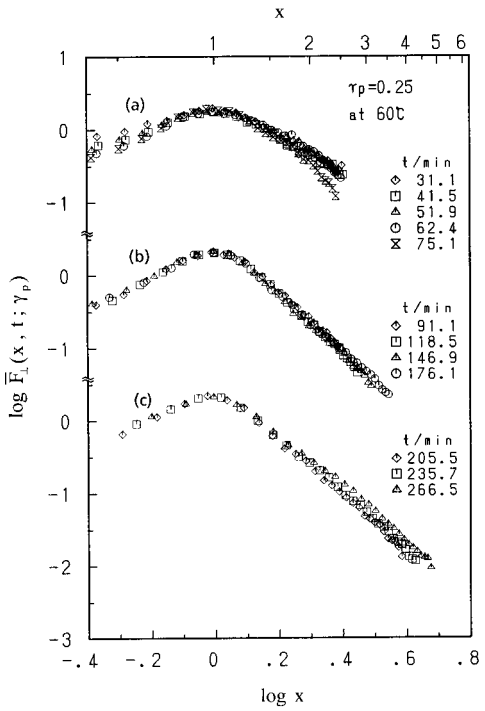

Figure 14. Reduced scaled structure factor $\bar{F}_\perp(x)$ on a double logarithmic scale at 60 °C with $x \equiv q/q_{m\perp}$ for the film with $\gamma_p = 0.25$.

at $x > 2$ in part b is due to a narrowing of the interface thickness t_I (late stage I).[10] However, in the later part of the late stage (late stage II), $\bar{F}_\perp(x)$ becomes universal with t, even at $x > 2$, because the interface thickness relative to Λ_0 becomes negligibly small.[10]

Figure 14 shows the reduced scaled structure factor $\bar{F}_\perp(x)$ at $\gamma_p = 0.25$. Note that the scaled structure factor at 31.1 min in part a is the one obtained immediately after the compression. In parts b and c, the higher order maximum at $x \cong 3$ disappears (cf. Figures 13b and 14b), and the power law behavior $\bar{F}_\perp(x)$ at $1 < x < 2$ is found to change such that the exponent n changes from -3 to -4 at an earlier time after the uniaxial compression (at a time between 62 and 75 min in part a in this figure). The curious change of the x-dependence of the $\bar{F}_\perp(x)$ seems to originate from generation of the new concentration fluctuations with high-q modes and their growth. The scaled structure factors at later stages (curve b to c) are essentially identical to that of the undeformed case (part b to c) in Figure 13). Thus, in the time domain covered by parts b and c, the uniaxial compression appears to change only the characteristic wave number $q_{m\perp}(t)$ and $q_{m\parallel}(t)$: after the compression the domain structures grow with the dynamical self-similarity and the structures grown are statistically identical to those grown in the absence of the deformation (result 8). Note that the time t_{comp} beyond which the evolution of $q_{m\perp}(t;\gamma_p=0.25)$ is equal to that of $q_{m\perp}(t;\gamma_p=1)$ is 172 min. This was judged from a global parameter $q_{m\perp}(t;\gamma_p)$ in Figure 9. Therefore, in the time domain covered in part c, the memory effect of the uniaxial compression on the characteristic wave number has essentially decayed. A closer observation of the scaled structure factor, however, shows the following feature associated with local structures such as the interface; i.e., the scaled structure factor for the compressed specimen at $x > 1.5$ is slightly smaller in the intensity than that for the undeformed case. This implies that the interface thickness relative to the domain size is slightly greater for the compressed specimen than that for the undeformed specimen. Thus, the uniaxial compression tends to affect the interface structure perpendicular to the compression axis (result 9). In fact the intensity of $\bar{F}_\perp(x)$ at $x > 1.5$ tends to increase at a long time covered in part c, indicating that the narrowing of the interface thickness occurs effectively on this time scale.

V. Conclusion

Light scattering experiments have been performed on the phase-separation process of binary mixture of SBR and PB subjected to uniaxial compression as a function of compression ratio γ_p. The scattering profile was observed as a function of scattering vectors perpendicular to the compression axis. Immediately after the compression of the film which was first homogenized and then demixed at 60 °C for 31 min, the scattering vector $q_{m\perp}(\gamma_p)$ at the maximum intensity shifts toward smaller q, essentially according to isochoric affine deformation. Thus, the characteristic length changes according to the affine deformation with the compression. It is also shown that the structures as a whole tend to deform affinely. The reduced integrated intensity of the scattering function $Q_\perp(\gamma_p)/\gamma_p$ was almost constant against various γ_p covered in our experiments, indicating that the mean-squared refractive index fluctuation $\langle\eta^2\rangle$ was hardly changed by the uniaxial compression.

In the phase-separation process after the uniaxial compression, the time change in the scattering vector $q_{m\perp}(t;\gamma_p<1)$ at the maximum scattering intensity was considerably slowed: in the case of $\gamma_p = 0.25$, it remains unchanged for a while after the compression. As time elapses $q_{m\perp}(t;\gamma_p)$ approaches $q_{m0}(t)$, the time change in the characteristic wave number in the absence of the compression, indicating the memory effect of the uniaxial compression on $q_{m\perp}(t;\gamma_p)$ eventually decays with time. On the other hand, the time evolution of the peak scattered intensity $I_{m\perp}(t;\gamma_p)$ was not affected by γ_p. This is because the changes in $\langle\eta^2\rangle$, $q_{m\perp}{}^{-2}q_{m\parallel}{}^{-1}$, and $S_\perp(x)$ with time are hardly affected by the compression. In an earlier time after the uniaxial compression, the exponential growth of $I_\perp(q,t;\gamma_p)$ with time was apparently observed. The time domain where the linearized theory of eq 29 is applicabe expanded with an increased degree of the compression. Cahn's linear analysis revealed the following nonlinear effects on the growth of the fluctuations after the compression: (i) the growth rate of the modes of the fluctuations newly developed after the compression, especially in the high-q range ($q > q_{m\perp}$), strongly couples with that of the dominant mode of the fluctuations with the wave number $q_{m\perp}(\gamma_p)$ existing right after the compression; (ii) the growth rate $R(q;\gamma_p)$ of the fluctuations at various q strongly depends on γ_p, i.e., the initial concentration fluctuations existed immediately after the compression.

The scaled structure factor was determined as a function of γ_p. The scaled structure factor for the compressed film is essentially identical to that of the undeformed case, especially at q satisfying $q/q_m \leq 2$. Even after the compression, the domains grow with the dynamical self-similarity. The structures are statistically identical to those grown in the absence of the deformation and therefore bicontinuous as clarified in our earlier studies.[8,9] However, the local structure factor related to the interface of the phase-separating domains was affected by a large uniaxial compression (e.g., $\gamma_p = 0.25$); the large compression tends to increase the interface thickness.

Acknowledgment. The authors express their thanks to Japan Synthetic Rubber Co. Ltd. for providing the samples. This work was partially supported by scientific grants from Japan Synthetic Rubber Co. Ltd. and Yokohama Rubber Co. Ltd. Japan.

References and Notes

(1) See, for example: Hashimoto, T. In *Current Topics in Polymer Science*; Ottembrite, R. M., Utracki, L. A., Inoue, T., Eds.; Hanser: Munich, New York, 1986; Vol. II, pp 199−242. Hashimoto, T. *Phase Transitions* **1988**, *12*, 47. Hashimoto, T. Structure and Properties of Polymers. In *Material Science and Technology*; Cahn, R. W., Haasen, P., Kramer, E. J., Eds.; Thomas, E. L., Vol. Ed.; VCH: Weinheim, Germany, 1993; Vol. 12, Chapter 6.

(2) Cahn, J. W.; Hilliard, J. E. *J. Chem. Phys.* **1958**, *28*, 258. Cahn, J. W. *J. Chem. Phys.* **1965**, *42*, 93. de Gennes, P. G. *J. Chem. Phys.* **1980**, *72*, 4756. Cook, H. E. *Acta Metall.* **1970**, *18*, 297.

(3) Hashimoto, T.; Itakura, M.; Hasegawa, H. *J. Chem. Phys.* **1986**, *85*, 6118. Hashimoto, T.; Itakura, M.; Shimidzu, N. *J. Chem. Phys.* **1986**, *85*, 6773.

(4) Jinnai, H.; Hasegawa, H.; Hashimoto, T.; Han, C. C. *J. Chem. Phys.* **1993**, *99*, 4845, 8145.

(5) Hashimoto, T.; Izumitani, T.; Takenaka, M. *Macromolecules* **1989**, *22*, 2293.

(6) Izumitani, T.; Hashimoto, T. *J. Chem. Phys.* **1985**, *83*, 3694.

(7) Izumitani, T.; Takenaka, M.; Hashimoto, T. *J. Chem. Phys.* **1990**, *92*, 3213.

(8) Takenaka, M.; Hashimoto, T.; Kawakatsu, T.; Kawasaki, K. *Phys. Rev. E* **1995**, *52*, 2247.

(9) Takenaka, M.; Izumitani, T.; Hashimoto, T. *J. Chem. Phys.* **1990**, *92*, 4566.

(10) Hashimoto, T.; Takenaka, M.; Jinnai, H. *J. Appl. Crystallogr.* **1991**, *24*, 457. Takenaka, M.; Hashimoto, T. *J. Chem. Phys.* **1992**, *96*, 6177.

(11) Binder, K.; Stauffer, D. *Phys. Rev. Lett.* **1974**, *33*, 1006.

MA960264Z